Towards Real-Time 3D Modeling of Induction Logs Using an Integral Equation Method

Saputera, D.H.; Jakobsen, M.; Jahani, N.; Alyaev, S.; Eikrem, K.S.; van Dongen, K.W.A.

DOI
10.3997/2214-4609.202310505

Publication date
2023

Document Version
Final published version

Citation (APA)
Saputera, D. H., Jakobsen, M., Jahani, N., Alyaev, S., Eikrem, K. S., & van Dongen, K. W. A. (2023). *Towards Real-Time 3D Modeling of Induction Logs Using an Integral Equation Method*. Paper presented at 84th EAGE ANNUAL Conference and Exhibition 2023, Vienna, Austria. https://doi.org/10.3997/2214-4609.202310505

2023 EAGE ANNUAL
84TH CONFERENCE & EXHIBITION
VIENNA | AUSTRIA

Towards Real-Time 3D Modeling of Induction Logs Using an Integral Equation Method

D.H. Saputera[1], M. Jakobsen[1], N. Jahani[2], S. Alyaev[2], K.S. Eikrem[2], K.W.A. Van Dongen[3]

[1] University Of Bergen; [2] NORCE Norwegian Research Centre; [3] Delft University of Technology

Summary

Real-time 3D imaging of the induction log is essential for improving the decision-making process in geosteering. To fulfill this need, we investigated various strategies for reducing the computational cost for 3D modelling of induction logs using the integral equation (IE) method, including the use of iterative Krylov solver, convolution with FFT algorithm, contraction IE formulation, computation acceleration with GPUs, and domain decomposition. We present two cases example to demonstrate the implementation of IE with these strategies. In the first case, we show that the application of domain decomposition allows one to only discretize the inhomogeneous domain and save the computation cost in the case of isolated domains. We present a logging while drilling scenario on a complex model for the second case. Our implementation of the efficient IE on GPUs enables significant acceleration and allows the computation of 3D forward modelling within less than two minutes for each local 3D simulation domain with approximately two million grid cells on a laptop. The implementation of domain decomposition formulation shows a different arrangement of solving IE by decomposing the domain.

Towards Real-Time 3D Modelling of Induction Logs Using an Integral Equation Method

Introduction

A typical tri-axial borehole electromagnetic (EM) induction tool has multiple axial components with different sensitivities. Together, they can capture the presence of anisotropy in the medium related to the formation's petrophysical properties. Full three-dimensional (3D) modelling of induction logs is required to image complex geological formations (Puzyrev et al., 2019). Having this geological structural information in real-time from 3D inversions of induction logs is important for adequate geosteering in order to achieve better well placement, completion, and production (Wilson et al., 2019). In practice, 3D inversion is challenging due to the large computational cost required for the 3D forward modelling, especially when quantification of the uncertainties in the inversion is required. Therefore, a fast 3D forward solver that accurately models induction logs is essential for the development and testing of new imaging methods.

In this study, we have investigated various strategies for reducing the computational cost for 3D modelling of induction logs using the integral equation (IE) method, including the use of iterative Krylov solver, convolution with FFT algorithm, contraction IE formulation, computation acceleration with GPUs, and domain decomposition. Discretization of the IE leads to a linear system that can be efficiently solved using iterative Krylov subspace methods (Fang et al., 2006). A FFT algorithm is utilized for computing the convolution of the contrast source with the dyadic Green's function to increase the computational efficiency (Fang et al., 2006). The use of the contraction integral equation formulation in Hursán and Zhdanov (2002) ensures the convergence of the iterative solver and improves the iterative solver efficiency for any resistivity contrast and any strength of the anisotropy. In addition, the implementation of the IE method on GPUs further increases computational efficiency. The high number of cores available on a GPU enables the acceleration of mathematical operations that can be straightforwardly parallelized (Dyatlov et al., 2015). With the domain decomposition formulation proposed by (Endo et al., 2009), it is possible to decompose the spatial domain into multiple anomalous domains and still enable FFT implementation without including the homogeneous part between the domains.

To illustrate the power and flexibility of the different strategies that we investigated, we present two case examples in this article. The first case is our implementation of the domain decomposition (DD) on an induction logging case with the presence of two isolated anomalous domains. We show that the modelling of induction logs in the subsurface can also take the computational advantage of DD, which is originally developed for large-scale surface EM modelling. In the second case, we present a logging while drilling scenario on a complex model inspired by a real geosteering scenario on the Norwegian Continental Shelf. In this case, we use a local 3D simulation domain, with a source at the origin, that is moved along the drilling trajectory. We assume that the interaction between the scatterers inside and outside of the local simulation domain is small and can be ignored. Our implementation of the efficient IE on GPUs enables significant acceleration and allows the computation of 3D forward modelling within less than two minutes per local 3D simulation domain with approximately two million grid cells.

Theory

The Maxwell's Equation. The modelling of induction tools response is governed by the inhomogeneous Maxwell's equation in the frequency domain (Zhdanov, 2009), viz.

$$\nabla \times \mathbf{E}(\mathbf{r}) = i\omega\mu_0\mathbf{H}(\mathbf{r}) - \mathbf{j}^{\mathbf{m}}, \quad (1)$$

$$\nabla \times \mathbf{H}(\mathbf{r}) = \hat{\boldsymbol{\sigma}}\mathbf{E}(\mathbf{r}) + \mathbf{j}^{\mathbf{e}}, \quad (2)$$

where $\mathbf{E}(\mathbf{r})$ and $\mathbf{H}(\mathbf{r})$ are the total electric and magnetic fields, respectively, at location $\mathbf{r}$. $\mathbf{j}^{\mathbf{e}}$ and $\mathbf{j}^{\mathbf{m}}$ denote electric and magnetic sources respectively. ω is the angular frequency, μ_0 is the magnetic permeability of free space, $\boldsymbol{\varepsilon}$ is the dielectric permittivity, $\hat{\boldsymbol{\sigma}} = \boldsymbol{\sigma} - i\omega\boldsymbol{\varepsilon}$ is the complex conductivity, and $i = \sqrt{-1}$. Under the low frequency approximation, the imaginary part of the complex conductivity is ignored.

Integral Equation Method. The total electric and magnetic fields can be formulated using the following integral equations (Fang et al., 2006)

$$\mathbf{E}(\mathbf{r}) = \mathbf{E^0}(\mathbf{r}) + \int_V \mathbf{G_E^0}(\mathbf{r},\mathbf{r}')\,\Delta\boldsymbol{\sigma}(\mathbf{r}')\mathbf{E}(\mathbf{r}')\,\mathrm{d}\mathbf{r}'^{\mathbf{3}}, \tag{3}$$

$$\mathbf{H}(\mathbf{r}) = \mathbf{H^0}(\mathbf{r}) + \int_V \mathbf{G_H^0}(\mathbf{r},\mathbf{r}')\,\Delta\boldsymbol{\sigma}(\mathbf{r}')\mathbf{E}(\mathbf{r}')\,\mathrm{d}\mathbf{r}'^{\mathbf{3}}, \tag{4}$$

where the 0 superscripts indicate the fields and Green's tensors defined for an isotropic homogeneous background medium with conductivity σ_0 due to a magnetic source. We choose a homogeneous isotropic background medium for simplicity and efficiency when calculating the Green's function (Fang et al., 2006). The tensor $\Delta\boldsymbol{\sigma}(\mathbf{r}') = \boldsymbol{\sigma} - \sigma_0\mathbf{I}$, denotes the conductivity contrast between the actual anisotropic medium and the background medium, and with $\mathbf{I}$ the identity tensor. The electric Green's tensor $\mathbf{G_E^0}$ and its relation to the magnetic Green's tensor $\mathbf{G_H^0}$ are (Fang et al., 2006)

$$\mathbf{G_E^0} = \left(\mathrm{i}\omega\mu_0\,\mathbf{I} + \frac{\nabla\nabla}{\sigma^0}\right)\mathrm{g}(\mathbf{r},\mathbf{r}'), \text{ and } \mathbf{G_H^0} = (\mathrm{i}\omega\mu_0)^{-1}\nabla\times\mathbf{G_E^0}, \tag{5}$$

where $\mathrm{g}(\mathbf{r},\mathbf{r}') = \frac{\mathrm{e}^{\mathrm{i}k_0|\mathrm{r}-\mathrm{r}'|}}{4\pi|\mathrm{r}-\mathrm{r}'|}$ is the scalar Green's function and with $k_0^2 = \mathrm{i}\omega\mu_0\sigma_0$. To calculate the total magnetic fields, the total electric fields need to be obtained first by solving equation (3). Afterward, the calculation of the total magnetic fields is a straightforward addition of background magnetic fields with the integral term.

Linear Systems of IE. From the discretization of equation (3), we obtain a linear system of equations that can be expressed in operator form as

$$\left(\mathbf{I} - \mathbf{G_E^0 V}\right)\mathbf{E} = \mathbf{E^0}, \tag{6}$$

where $\mathbf{G_E^0 V}$ is the tensor that represents the convolution integral of the Green's tensor with the contrast source and $\mathbf{V}$ is the tensor of the discretized contrast $\Delta\boldsymbol{\sigma}(\mathbf{r}')$. The linear system in equation (6) can be efficiently solved using the Krylov subspace iterative method. In this study, we use the biconjugate stabilized solver or BiCGSTAB (van der Vorst, 1992).

Convolution with FFT. At each step of the iterative solver, the convolution integral of the dyadic Green's function can be efficiently calculated using FFT

$$\mathbf{G_E^0 VE} = \mathcal{F}^{-1}\left(\mathcal{F}\left(\mathbf{G_E^0}\right)\odot\mathcal{F}(\mathbf{VE})\right), \tag{7}$$

where $\mathcal{F}$ is the FFT operator and $\odot$ denotes elementwise multiplication. The FFT of the Green's tensor can be pre-calculated to save computational time during the iterative process.

Contraction IE. Hursán and Zhdanov (2002) described the contraction integral equation that ensures convergence and increases the rate of convergence in the presence of high contrast. By applying pre-conditioners, equation (6) becomes

$$\mathbf{M_1 A M_2}\left(\mathbf{M_2^{-1}E}\right) = \mathbf{M_1 E^0}, \tag{8}$$

where $\mathbf{A} = \mathbf{I} - \mathbf{G_E^0 V}$, $\mathbf{M_1} = \sqrt{\mathrm{Re}\,\sigma_0}$, and $\mathbf{M_2} = 2\sqrt{\mathrm{Re}\,\sigma_0}(2\mathrm{Re}\,\sigma_0\mathbf{I} + \mathbf{V})^{-1}$. The new linear system in equation (8) is solving for the scaled electric field $\mathbf{M_2^{-1}E}$. It has better convergence properties because the contraction Green's operator norm is always less than or equal to one. Consequently, the condition number of $\mathbf{M_1 A M_2}$ is lower than the original integral operator $\mathbf{A}$.

Domain Decomposition (DD). Adapting the DD formulation described in Jakobsen and Tveit (2018), the electric field $\mathbf{E}$ and conductivity contrast $\mathbf{V}$ at the location $\mathbf{r}$ with non-zero contrast can be expressed as the sum of non-overlapping $\mathbf{E}$ and $\mathbf{V}$. For N number of domains, we can write

$$\mathbf{E} = \sum_{\mathbf{i=1}}^{\mathbf{N}}\mathbf{E_i}, \text{ and } \mathbf{V} = \sum_{\mathbf{i=1}}^{\mathbf{N}}\mathbf{V_i}, \tag{9}$$

where $\mathbf{E_i}$ and $\mathbf{V_i}$ are defined to be zero outside of domain i. Substituting (9) into equation (6) yields N linear systems of equations at each domain

$$\left(\mathbf{I} - \mathbf{G_{ii}^0 V_i}\right)\mathbf{E_i} = \mathbf{E_i^0} + \sum_{\mathbf{j=1,j\neq i}}^{\mathbf{N}}\mathbf{G_{ij}^0 V_j E_j}, \text{ i=1,2,…,N} \tag{10}$$

where $\mathbf{G_{ij}^0 V_j E_j}$ is the electric field at domain i due to contrast source at domain j with $\mathbf{G_{ij}^0}$ are the intra-domain Green's operator for i = j and inter-domain Green's operator for i ≠ j. The linear systems that arise in the DD formulation can be solved in an iterative manner (Endo et al., 2009) with the sum of the interaction terms on the right-hand side of the equation (10) assumed to be zero in the first step.

Numerical Examples and Discussion

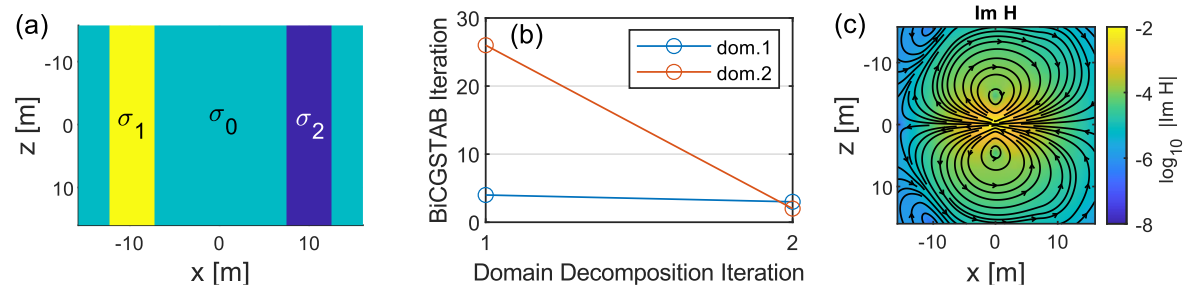

Figure 1 *(a) Two anomalous domains on a homogeneous background. (b) BiCGSTAB solver convergence at each DD iteration. (c) Imaginary part of the calculated H-field.*

Two Isolated Domains. The center of the anomalous domains in Figure 1a are 20 m apart and both anomalous domains have an equal size of 5 x 32 x 32 m^3 (cell size = 0.25 x 0. 25 x 0. 25 m^3) with $\sigma_0 =$ 0.5 S/m, $\sigma_1 = 1$ S/m, and $\sigma_2 = 0.05$ S/m. This model is simulated with a source frequency of 24 kHz at the origin and oriented in the x-direction. Figure 1b shows that the desired convergence is achieved within two DD iterations which indicates low interaction between domains. Also, the number of BiCGSTAB iterations indicates different convergence rates at different domains. In this case, the IE with DD is approximately two times faster than solving the full domain (32 x 32 x 32 m^3) within the same numerical error level. This is due to the computational saving of having a smaller number of discretized cells. Both IE with DD and full domain are showing the same magnetic field pattern as shown in Figure 1c with an average magnitude difference of less than 0.001%.

Faulted Anisotropic Model. To test our approach on complex media, we simulated induction logs across faulted anisotropic formation for a 48 kHz source frequency and an 85° drilling angle as illustrated in Figure 2a. The subsurface resistivity value is assigned according to the color code in Figure 2a and does not vary in the y-direction. We use a moving local 3D simulation domain with a source at the origin to simulate the whole model, assuming the contribution of the contrast sources outside of the domain is small and can be ignored. The local simulation domain is discretized into 128 x 128 x 128 cells and a cell size of 0.38 x 0.38 x 0.38 m^3. The local simulation domain axes are rotated according to the drilling angle and it is moved along the drilling trajectory from the starting point (0, -32.48) to the endpoint (1172.5, 70.1). Following Fang et al. (2006), we set a constant background conductivity $\sigma_0 = \sqrt{\min(\sigma)\max(\sigma)} = \sqrt{(1/1.5) * (1/50)} = 0.1155$ S/m for all local simulations.

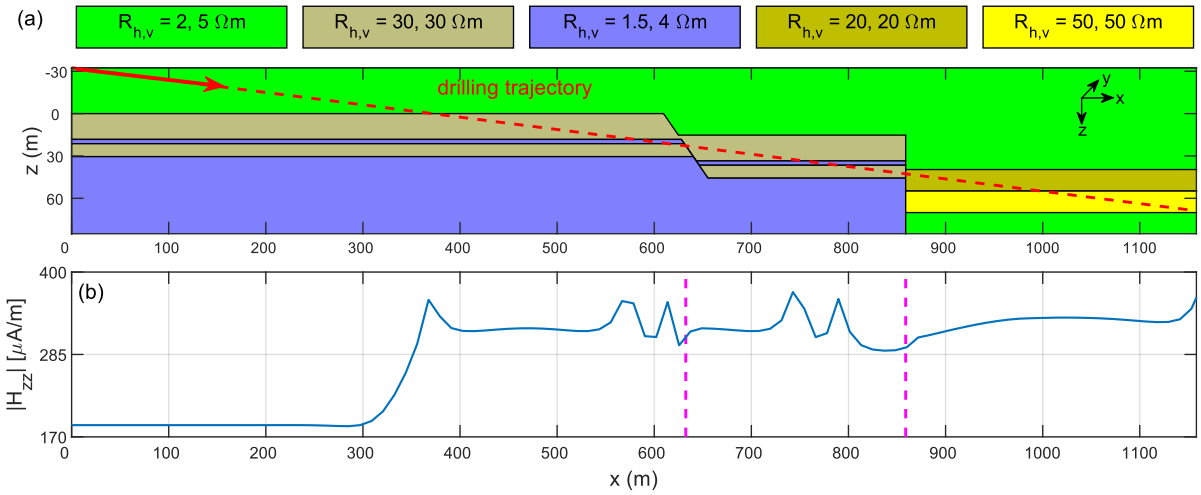

Figure 2 *(a) Sketch of the 2.5D model and the drilling trajectory. (b) Magnitude of H_{zz} component of the induction log.*

Figure 2b shows the magnitude of H_{zz} components at a receiver with spacing 7.62 m from the source. The magenta dashed lines indicate the crossing of the drilling trajectory and the faults. We simulated 100 logging positions and the time for calculating 9 coupling components (3 source orientations) in one logging position is within the range of 30 s to 60 s. Because we use a homogeneous isotropic background, the anomalies are everywhere inside the local simulation domain and no computational saving was made by simply decomposing the local domain into two domains in the y-direction. In this case, more advanced domain decomposition needs to be investigated. The simulations are executed on a laptop with AMD Ryzen 7 4800H CPU and NVIDIA GeForce RTX 3060 Laptop GPU. We have compared the simulation results of our IE implementation with Finite Difference code for an anisotropic layered model and the result agrees within a 2% difference (Saputera D.H. et. al., 2022).

Concluding Remarks

The combination of an efficient IE implementation and taking advantage of GPU acceleration enables the modelling of a logging while drilling case with approximately $2x10^6$ simulation cells at each logging position within 30 s – 60 s on a simple laptop. The domain decomposition formulation allows one to save computational time by discretizing only at the inhomogeneous domain and we observed two times faster computation on the isolated domain case. Although no savings were observed on the complex media, the DD formulation shows a different arrangement of solving IE. In future work, we aim to investigate the more advanced implementation of DD to improve the discretization of the IE method.

Acknowledgements

This work is part of the Center for Research-based Innovation DigiWells: Digital Well Center for Value Creation, Competitiveness and Minimum Environmental Footprint (NFR SFI project no. 309589, https://DigiWells.no). The center is a cooperation of NORCE Norwegian Research Centre, the University of Stavanger, the Norwegian University of Science and Technology (NTNU), and the University of Bergen. It is funded by Aker BP, ConocoPhillips, Equinor, Lundin Energy, TotalEnergies, Vår Energi, Wintershall Dea, and the Research Council of Norway.

References

Dyatlov, G., Onegova, E., and Dashevsky, Y. [2015]. Efficient 2.5D electromagnetic modeling using boundary integral equations. *GEOPHYSICS*, **80**(3), E163–E173.
Endo, M., Čuma, M., and Zhdanov, M. S. [2009]. Large-scale Electromagnetic Modeling for Multiple Inhomogeneous Domains. *Communications in Computational Physics*, **6**(2), 269–289.
Fang, S., Gao, G., and Verdin, C. T. [2006]. Efficient 3D Electromagnetic Modelling in the Presence of Anisotropic Conductive Media, Using Integral Equations. *Exploration Geophysics*, **37**(3), 239–244.
Hursán, G., and Zhdanov, M. S. [2002]. Contraction integral equation method in three-dimensional electromagnetic modeling. *Radio Science*, **37**(6), 1-1-1–13.
Jakobsen, M., and Tveit, S. [2018]. Distorted Born iterative T-matrix method for inversion of CSEM data in anisotropic media. *Geophysical Journal International*, **214**(3), 1524–1537.
Puzyrev, V., Pardo, D., Calo, V., and Torres-Verdín, C. [2019]. Recent advances on the inversion of deep directional borehole resistivity measurements. *ASEG Extended Abstracts*, *2019*(1), 1–3.
Saputera D.H., Jakobsen M., Jahani N., Alyaev S., Eikrem K.S., van Dongen K.W.A. [2022]. GPU-accelerated integral equation method for 3D modelling of induction logs. [Poster]. *Geosteering and Formation Evaluation Workshop by NORCE, Stavanger, Norway, 1-2 November 2022*. https://nfes.org/2022/10/14/gpu-accelerated-workshop-abstract-23.html
van der Vorst, H. A. [1992]. Bi-CGSTAB: A Fast and Smoothly Converging Variant of Bi-CG for the Solution of Nonsymmetric Linear Systems. *SIAM Journal on Scientific and Statistical Computing*, **13**(2), 631–644.
Wilson, G., Marchant, D., Haber, E., Clegg, N., Zurcher, D., Rawsthorne, L., and Kunnas, J. [2019]. Real-Time 3D Inversion of Ultra-Deep Resistivity Logging-While-Drilling Data. *SPE Annual Technical Conference and Exhibition*. OnePetro.
Zhdanov, M. S. [2009]. *Geophysical electromagnetic theory and methods*. Elsevier.